Hydrol. Earth Syst. Sci., 30, 3529–3547, 2026
https://doi.org/10.5194/hess-30-3529-2026

Hydrology and Earth System Sciences
Open Access
EGU

Projections of future hydrological drought in a reservoir-regulated region: the roles of climate change and reservoir operation

Shaokun He[1,4,5], Sirui Sun[2], Yanghe Liu[3], Kebing Chen[1], Lingling Zhu[1], and Yu Gong[5]

[1]Bureau of Hydrology, Changjiang Water Resources Commission, Wuhan 430010, China
[2]Middle Changjiang River Bureau of Hydrology and Water Resources Survey, Bureau of Hydrology of Changjiang Water Resources Commission, Wuhan 430010, China
[3]Three Gorges Cascade Dispatch & Communication Center, China Yangtze Power Co., Ltd., Yichang 443000, China
[4]Department of Earth and Environmental Sciences, Lund University, Lund 223 62, Sweden
[5]State Key Lab. of Water Resources Engineering & Management, Wuhan University, Wuhan 430072, China

Correspondence: Kebing Chen (chenkb@whu.edu.cn) and Yu Gong (ygong@whu.edu.cn)

Received: 8 November 2025 – Discussion started: 24 November 2025
Revised: 15 May 2026 – Accepted: 29 May 2026 – Published: 11 June 2026

Abstract. Future hydrological droughts in reservoir-regulated regions remain uncertain due to the complex interactions between climate change and reservoir operation. Existing studies usually rely on simplified empirical representations of historical reservoir operations and rarely consider the role of optimal reservoir operation policies. Here, we used the upper Hanjiang River basin (UHRB) in China as a case study to project its future hydrological drought evolution using standard streamflow indices (i.e., SSI-1, SSI-3, and SSI-12) and to quantify the roles of climate change and reservoir operation. A long short-term memory (LSTM)-based hydrological model, coupled with a physics-informed LSTM reservoir model, was developed and driven by bias-corrected climate outputs from five global climate models to project future drought conditions under three scenarios (SSP126, SSP370, and SSP585). The results indicate that future climate change over the UHRB is projected to reduce natural streamflow and exacerbate hydrological droughts, with the most severe impacts projected in the far-future period (2071–2100) under SSP585. The traditional Ankang Reservoir operation reduces the frequency, duration and severity of short-term hydrological droughts (SSI-1 and SSI-3) under all scenarios, but shows limited effectiveness for long-term droughts (SSI-12). Importantly, optimal reservoir operating policies that aim to maximize hydropower generation and power generation guarantee rate reveal clear trade-offs between hydrological drought risk and hydropower benefits, thereby underscoring the importance of enhancing reservoir operation strategies for future drought management in reservoir-regulated basins.

1 Introduction

Hydrological droughts, characterized by abnormally low streamflow in rivers, have significant direct and indirect ramifications on hydrological, agricultural, and socio-economic sectors, such as losses in crop production and hydropower generation (Chang et al., 2025; Ji et al., 2023; Kheyruri et al., 2023). In recent decades, hydrological droughts have become more frequent in the Americas, East Asia, Africa, and Oceania, and global warming arising from high greenhouse gas concentrations has been identified as the main driver (Gudmundsson et al., 2021). According to the Sixth Assessment Report (AR6) of the Intergovernmental Panel on Climate Change (IPCC, 2021), land temperatures are projected to continue to rise, which is expected to exacerbate extreme hydrological droughts in a warming future. Hence, it is of great importance to assess the characteristics of extreme hydrological droughts in the context of climate change to enable effective adaptation strategies.

At the same time, the rapid global expansion of reservoirs as a major manifestation of human intervention in river systems has introduced new challenges for assessing future hydrological droughts. Currently, more than 55 000 reservoirs have been registered by the International Commission

on Large Dams, with a total storage capacity of 14 602 km^3 (Eriyagama et al., 2020). Such an extensive storage capacity suggests that reservoirs can substantially affect hydrological drought characteristics by regulating the spatiotemporal distribution of river flows (Ho and Ehret, 2025; G. Ribeiro Neto et al., 2023). From the perspective of hydraulic regulation alone, reservoirs are often found to dampen low-flow extremes in strongly regulated river basins, particularly in Europe and North America, thereby alleviating drought severity during dry seasons (Wanders and Wada, 2015). However, reservoirs also enable intensified consumptive water use, including irrigation expansion and other anthropogenic withdrawals, which may counteract or even outweigh the buffering effects of flow regulation. For example, Wan et al. (2018) reported that irrigation reservoirs could increase the duration and intensity of global hydrological droughts by up to 50 % during 2070–2099, largely due to enhanced water abstractions. Consequently, the net impact of reservoir operation on future hydrological droughts is highly region-dependent, reflecting the combined effects of hydraulic regulation, reservoir-enabled water use, and the heterogeneity of regional climate change.

Recently, some scholars have begun such drought analysis efforts in some key watersheds (Sun et al., 2023; Zhang et al., 2025; Cheng et al., 2024). Yun et al. (2021b) attempted to assess the effectiveness of reservoir operation in modifying hydrological extremes in the Lancang-Mekong River basin using five global climate models (GCMs) from the Coupled Model Intercomparison Project Phase 6 (CMIP6) and the VIC-Reservoir model. Ji et al. (2023) projected hydrological drought changes in the upper Yellow River basin under different levels of global warming by driving a hybrid Conjunctive Surface-Subsurface Process Version 2 (CSSPV2) hydrological model coupled with a conceptual reservoir model derived from Hanasaki et al. (2006), in which reservoir operations were represented using a generic rule-based formulation with empirically calibrated parameters. These drought experiments demonstrated the feasibility of coupling hydrological and reservoir modules for such problems, but their conclusions may remain sensitive to empirical assumptions about reservoir releases when observed operating records (i.e., inflow/release/storage time series) are not explicitly used to constrain or evaluate the operating representation. As one of the most influential human-engineered interventions under a changing climate, reservoir systems warrant particular attention regarding the extent to which realistic operating patterns can sustain system performance under plausible future scenarios (Culley et al., 2016). Historical operating records contain rich decision-making information that reflects how operators have adapted release strategies to diverse inflow conditions (Zheng et al., 2022). Therefore, state-of-the-art tools that can systematically learn from long-term historical operating records during periods with relatively stable objectives and constraints are critical for capturing drought-relevant reservoir releases.

Against this background, machine learning (ML) offers a promising complementary approach to reproducing historical reservoir operation processes. A range of data-driven ML models, including artificial neural networks (ANN) (Özdoğan-Sarıkoç et al., 2023), nonlinear autoregressive models with exogenous input (NARX) (Yang et al., 2019), and long short-term memory (LSTM) networks (Tran et al., 2025), have been applied to simulate reservoir operations using large-sample historical records. Among them, LSTM-based models have demonstrated particularly favorable performance. Embedding physical mechanisms or operational constraints can further enhance their ability to represent operational behaviors under hydrological extremes, thereby allowing for a more accurate representation of high- and low-flow dynamics (Zheng et al., 2022). Building on this line of research, coupling an LSTM-based reservoir operation module with an LSTM-based hydrological process model can offer a pathway towards an integrated data-driven framework for more automated drought diagnosis. This direction is motivated by key limitations of traditional process-based hydrological models (e.g., VIC and CSSPV2), including their reliance on basin-specific calibration and substantial requirements for physiographic inputs and parameterization (e.g., topography, land use, and soil properties), which together constrain model transferability across regions (Arsenault et al., 2023).

Beyond assessing how historical operating policies may shape future hydrological droughts, it is also crucial to examine how effective optimal operating policies are in balancing operating benefits against hydrological extremes. Optimal reservoir operation has been widely studied as a way to enhance water-resource benefits without additional capital investment (He et al., 2025; Wan et al., 2025). While some recent studies have incorporated drought-related performance metrics (e.g., water-supply deficits or reliability) into operational analyses and optimization frameworks (e.g., Huang et al., 2026), these approaches primarily reflect the impacts of dry conditions on water-supply performance rather than explicitly quantifying hydrological drought states using drought indices. Consequently, the literature has largely focused on conceptual analyses of the interplay between optimal reservoir operation and hydrological droughts, with limited evidence from systematic implementation and evaluation in real-world water-management practice (Huang et al., 2025; Ji et al., 2023). It therefore remains unclear whether embedding such optimal strategies into existing management regimes would ultimately strengthen or weaken basin-scale resilience to hydrological drought extremes under climate change.

Here, we aim to advance current reservoir-related drought assessment frameworks by (i) replacing traditional process-based hydrological models with a fully data-driven LSTM framework for hydrological drought quantification, and (ii) explicitly exploring the adaptive performance of optimal operating policies under future climate change. Using the upper

Hanjiang River basin in China, a heavily reservoir-regulated system, as a representative case, we investigate the relative and combined influences of climate change and reservoir operation on future hydrological droughts under three CMIP6 shared socioeconomic pathways. Specifically, we first develop a hybrid modelling framework that couples an LSTM-based hydrological model with a physics-guided LSTM reservoir operation model to reproduce historical inflow and release, respectively. The trained hybrid model is then driven by bias-corrected outputs from five CMIP6 GCMs to project daily streamflow under near- and far-future scenarios. Hydrological drought characteristics, including duration, frequency, and severity, are subsequently quantified using run theory for both historical and future periods. Finally, we explicitly assess how adopting optimized operating policies, in comparison with historical operating rules, may alter future hydrological drought characteristics and basin-scale drought resilience, thereby revealing the potential trade-offs between hydrological drought mitigation and operating benefits under a changing climate.

2 Study Area and Data Description

2.1 Study area

The Hanjiang River basin in central China plays a critical role in the regional water economy of riparian provinces. As the longest tributary of the Yangtze River, the basin has experienced extensive anthropogenic interventions, including the construction of a series of reservoirs and inter-basin water transfer projects. In particular, the Ankang Reservoir, a large reservoir situated near the outlet of the upper Hanjiang River basin (UHRB), exerts substantial control on downstream discharge. Its operation primarily influences a ~ 30 km reach immediately downstream (from the dam to the Ankang Hydrological Station), which we define as the regulated reach in this study. As shown in Fig. 1, the UHRB (31.0–34.5° N, 106.0–109.5° E) originates from the southern foothills of the Qinling Mountains and terminates at the Ankang Hydrological Station. The basin has a subtropical monsoon climate, with long-term mean annual precipitation, temperature, and runoff depth of approximately 850 mm, 15 °C, and 500 mm, respectively. The flood season (May–October) contributes about 75 % of annual precipitation, and streamflow exhibits a broadly similar seasonal pattern, indicating a high sensitivity to both flood and drought processes under the prevailing hydroclimatic regime (Jin et al., 2023).

With a total storage capacity of 3.2×10^9 m^3, the Ankang Reservoir is the largest and most downstream key control project within the UHRB. Commissioned in 1990, it is operated primarily for hydropower generation (installed capacity: 850 MW), while also serving flood control and navigation functions (Chinese National Committee on Large Dams, 2011). The reservoir controls a natural catchment area of about 35 700 km^2 and has an active storage capacity of 1.47×10^9 m^3 . We use discharge monitoring records collected at the reservoir upstream inlet and at the Ankang Hydrological Station, which represent inflow to the reservoir and regulated releases downstream, respectively.

2.2 Data

The research datasets used in this study include both historical in-situ observations and future climate projections. Historical meteorological records from eleven meteorological stations (Fig. 1) for the period 1992–2020 were obtained from the China Meteorological Administration Data Sharing Service Center (CMA, http://data.cma.cn, last access: 23 May 2025), including daily precipitation (Pr, mm), wind speed (Win, m s^{-1}), relative humidity (Rh, %), and air temperature (maximum, minimum, and mean; Tem, °). Basin-averaged precipitation and temperature time series were derived using the Thiessen polygon method. Observed streamflow data for the same historical period were obtained from the Bureau of Hydrology of the Yangtze Water Resources Commission of China (https://www.cjh.com.cn, last access: 23 May 2025). The inflow to the Ankang Reservoir can be regarded as near-natural flow with negligible anthropogenic disturbance.

For future climate projections, a multi-model ensemble was adopted, consisting of five GCMs under three Shared Socioeconomic Pathways (SSP126, SSP370, and SSP585), as listed in Table 1. Several previous studies have shown that raw CMIP6 climate variables (e.g., precipitation, air temperature) tend to be overestimated in Asia, with non-negligible uncertainties (Chai et al., 2022). To reduce systematic biases in climate model outputs, bias-corrected daily data from the Inter-sectoral Impact Model Intercomparison Project 3b (ISIMIP3b, https://data.isimip.org/search/tree/ISIMIP3b/InputData/, last access: 23 May 2025) were employed. These datasets were downscaled to a spatial resolution of $0.5° \times 0.5°$ using observational climate data and cover the period 1850–2100. In the bias-adjustment procedure, a trend-preserving parametric quantile mapping method was applied, accounting for interdependencies among different climate variables, thereby providing significant improvements over the previous ISIMIP2 framework (Lange, 2019). The robustness of ISIMIP3b has been demonstrated across many regions of China (Kang et al., 2023; Yun et al., 2021a; He et al., 2023). To assess climate change impacts, three equal 30-year periods were defined: the reference period (1985–2014), the near-future period (2031–2060), and the far-future period (2071–2100).

3 Methodology

This section presents the methodology for exploring future hydrological droughts under the coupled effects of cli-

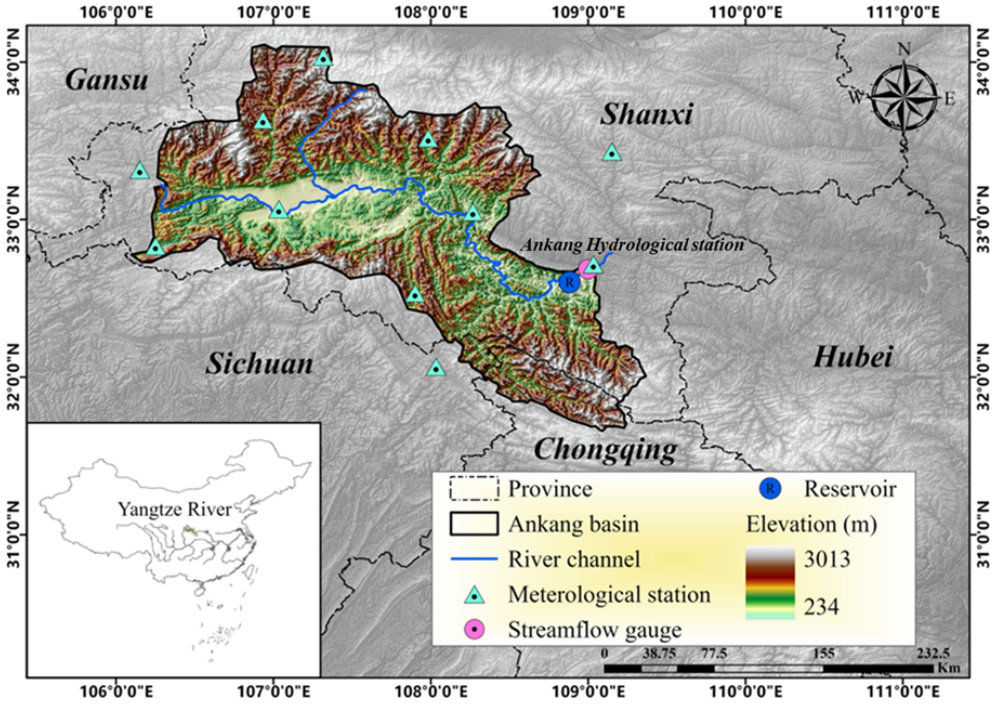

Figure 1. Location of the upper Hanjiang River Basin (UHRB) and key hydrological elements, showing the Ankang Reservoir and the downstream control section at the Ankang Hydrological Station. The reservoir-regulated reach analysed in this study extends ~30 km downstream from the dam to the station.

Table 1. Basic information on the five global climate models (GCMs) from ISIMIP3b.

ID	Model	Modeling Center (or Group)	Institution Name	Horizontal resolution (long × lat)
1	IPSL-CM6A-LR	IPSL	Institute Pierre Simon Laplace, France	2.50° × 1.27°
2	GFDL-ESM4	NOAA-GFDL	Geophysical Fluid Dynamics Laboratory, Princeton	1.25° × 1°
3	MPI-ESM1-2-HR	MPI-M	Max Planck Institute for Meteorology, Germany	0.9° × 0.9°
4	MRI-ESM2-0	MRI	Meteorological Research Institute, Japan	1.125° × 1.125°
5	UKESM1-0-LL	MOHC NERC	Met Office Hadley Centre and Natural Environment Research Council, UK	1.25° × 1.875°

mate change and reservoir operation, as illustrated in Fig. 2. First, an LSTM-based reservoir inflow simulation and a physics-based LSTM simulation for reservoir operation are performed. Then, the ISIMIP3b outputs are used to drive the hybrid modeling framework to project future streamflow scenarios and identify hydrological drought characteristics. Finally, a series of numerical experiments are designed to investigate the individual roles of climate change and reservoir operation in shaping future hydrological droughts. Each module is described in detail in the following subsections.

3.1 Long short-term memory (LSTM)

The LSTM is a variant of recurrent neural network that uses the backpropagation-through-time algorithm to address the vanishing gradient problem and retain information from earlier time steps (Hochreiter and Schmidhuber, 1997). It is specially structured with a gated memory block that introduces

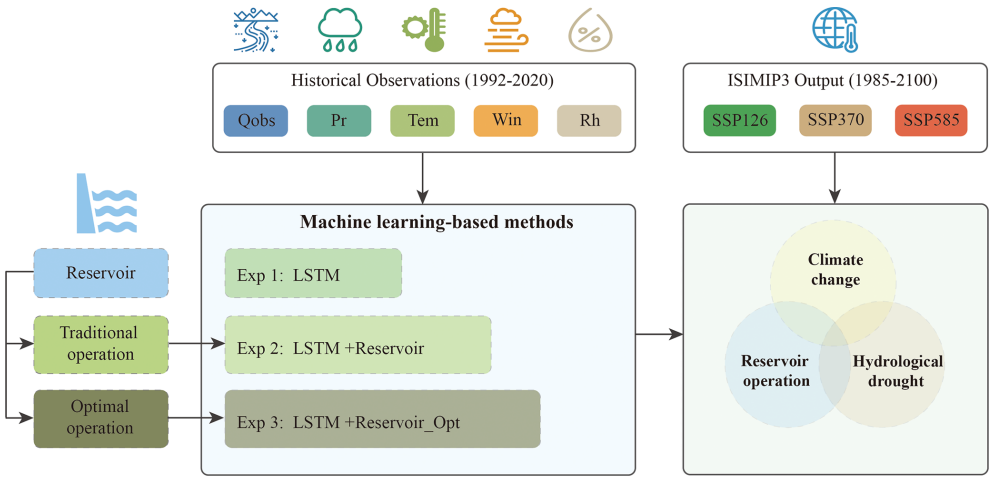

Figure 2. Schematic diagram of the modeling framework used to investigate the roles of climate change and reservoir operation in future hydrological droughts. The acronyms used in the experimental description panel are explained in Sect. 3.3.

a memory cell and gating mechanisms compared with conventional neural networks (Hochreiter, 1998; He et al., 2022; Chen and Yu, 2025). The memory block (shown in Fig. 3a) consists of a forget gate, an input gate, an output gate, and a memory cell. The forget gate determines which information from the previous cell state is discarded, whereas the input gate determines which information is used to update the cell state. The output gate then generates the hidden state based on the updated cell state. Mathematically, a typical memory block in an LSTM can be described by Eqs. (1) to (5).

$$f_t = \sigma(x_t W_f + h_{t-1} U_f + b_f) \quad (1)$$

$$i_t = \sigma(x_t W_i + h_{t-1} U_i + b_i) \quad (2)$$

$$o_t = \sigma(x_t W_o + h_{t-1} U_o + b_o) \quad (3)$$

$$c_t = f_t \otimes c_{t-1} + i_t \otimes \tanh(x_t W_c + h_{t-1} U_c + b_c) \quad (4)$$

$$h_t = o_t \otimes \tanh(c_t) \quad (5)$$

where x_t, f_t , i_t, and o_t denote the input variables, forget gate, input gate, and output gate at time t, respectively. c_t and h_t represent the cell state and the hidden state at time t, while c_{t-1} and h_{t-1} are their values at the previous time $t-1$. W, U and b with various subscripts denote input weights, recurrent weights and bias terms, respectively. $\sigma(\cdot)$ is the sigmoid activation function with a return value ranging from 0 to 1. $\tanh(\cdot)$ is the hyperbolic tangent activation function with a return value ranging from -1 to 1. $\otimes$ denotes element-wise multiplication.

3.1.1 LSTM-based reservoir inflow simulation

Some previous studies have shown that a three-layered LSTM with one hidden layer is sufficiently robust to capture nonlinear rainfall-runoff relationships, although the black-box nature of such models makes the interpretation of physical processes more challenging (Solanki et al., 2025; Rehana and Rajesh, 2023; Liu et al., 2022). Following these studies, a sequence-to-one LSTM architecture is adopted in this study to simulate near-natural reservoir inflow (Fig. 3b). The inputs to the LSTM consist of multiple meteorological variables, including precipitation, daily maximum and minimum air temperature, relative humidity, and wind speed, with selected lag times. The lag structure for each input variable is determined using cross-correlation analysis (Cui et al., 2022) to account for delayed hydrological responses and catchment memory effects. The model output is the near-natural reservoir inflow at time t. In addition to input selection, the number of hidden units and the initial learning rate are treated as key hyperparameters of the LSTM model. The hyperparameter tuning procedure is provided in Table S1 in the Supplement and was implemented using TensorFlow's Keras API (Abadi et al., 2016).

Notably, antecedent reservoir inflow is not included as an input variable in the LSTM model, although it is closely related to the target output in reality. This design choice is motivated by the difficulty of accurately predicting antecedent inflow under future climate scenarios, where such information can only be inferred from model simulations. Including antecedent inflow as an input may therefore introduce additional uncertainty and lead to an artificial accumulation of simulation errors. For historical simulations, meteorological data from 1992 to 2020 were used. The year 1992 was reserved as the model spin-up period to minimize the influence of initial conditions, while the remaining data were divided into a calibration period (1993–2014) and a validation period (2015–2020). Mean hydroclimatic conditions during the validation period were broadly comparable to those during the calibration period, with no pronounced wet or dry anomaly (He et al., 2023). Thus, the chronological split primarily evaluates temporal out-of-sample performance under similar historical conditions rather than transferability across con-

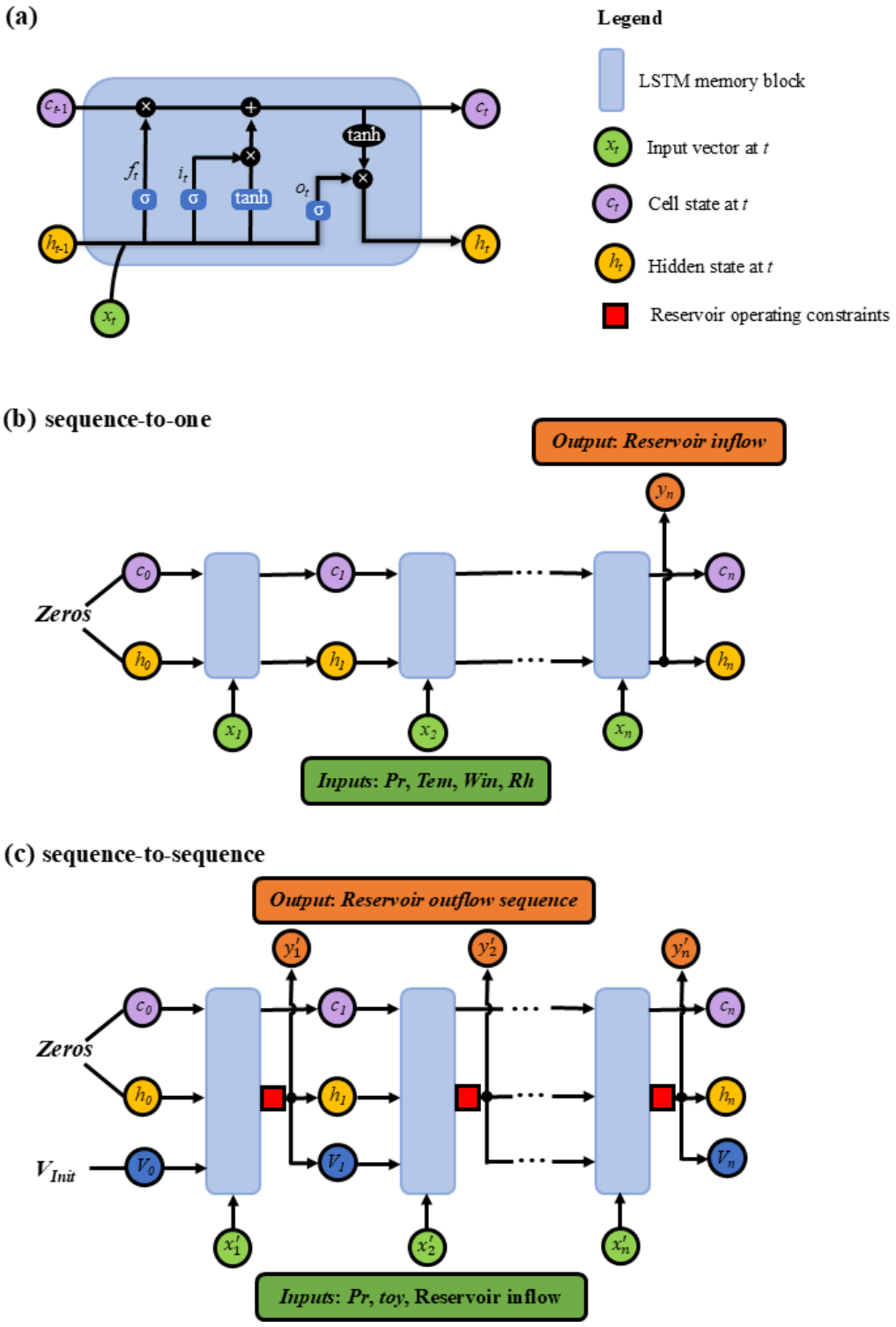

Figure 3. Model structure of the long short-term memory (LSTM). **(a)** Internal structure of a standard LSTM memory block, consisting of a forget gate, an input gate, an output gate, and a memory cell. **(b)** A three-layer sequence-to-one LSTM architecture driven by correlated meteorological inputs to simulate reservoir inflow. **(c)** A physics-guided LSTM-based sequence-to-sequence model with antecedent reservoir storage, time of year (toy), precipitation and simulated reservoir inflow as inputs to simulate reservoir release, where a red block following the LSTM block represents a set of operational constraints, including the water balance equation and reservoir storage and release limits.

trasting regimes. Model calibration was performed by maximizing the Nash–Sutcliffe efficiency (NSE; see Sect. 3.1.3 and Eqs. (9)–(10) using the Adam optimizer (Kingma and Ba, 2014). For future projections, the period 1985–2100 was used to cover the full simulation span of the SSP scenarios. Within this range, the period 1985–2014 was designated as the reference period, following ISIMIP3b protocol, to evaluate future streamflow variations against a consistent historical baseline. The calibration and validation periods are used exclusively for model training and evaluation, whereas the reference period is treated independently for climate impact assessment.

3.1.2 Derivation of historical operation patterns with a physics-guided LSTM model

For human-intervened reservoir operation, which often involves substantial expert knowledge, LSTM, as a state-of-the-art machine learning technique, has been shown to outperform traditional empirical approaches in learning operating rules from large historical records (Zheng et al., 2022; Longyang and Zeng, 2023; García-Feal et al., 2022). In contrast to the inflow simulation in Fig. 3b, we constructed a three-layer sequence-to-sequence LSTM model (Fig. 3c) to simulate reservoir release.

Following the guidelines of the local reservoir management agency, antecedent reservoir storage, time of year, precipitation, and reservoir inflow were used as the major inputs. To improve the robustness of the model for future simulations, we used the LSTM-simulated inflow from Sect. 3.1.1 rather than observed inflow records. In addition, a state variable representing reservoir storage was incorporated and initialized at the flood-limited water level, which can be updated via the state transition equation (i.e., the water balance equation in Eq. (6). To avoid physically unrealistic states during the simulation (e.g., violation of operational constraints), additional operational constraints, including reservoir storage limits in Eq. (7) and reservoir release limits in Eq. (8), were also incorporated, resulting in a physics-guided LSTM model.

$$V_{t+1} = V_t + (I_t - O_t) \cdot \Delta t \tag{6}$$

$$V_{\min} \le V_t \le V_{\max} \tag{7}$$

$$O_{\min} \le O_t \le O_{\max} \tag{8}$$

where V_t and V_{t+1} are the reservoir storage (m^3) at the beginning and end of time step t, respectively; I_t and O_t are the reservoir inflow ($m^3\,s^{-1}$) and release ($m^3\,s^{-1}$) at time t, respectively; $V_{\min}$ and $V_{\max}$ are the allowable minimum and maximum reservoir storage (m^3), respectively; $O_{\min}$ and $O_{\max}$ are the allowable minimum and maximum reservoir release ($m^3\,s^{-1}$), respectively; and Δt is the simulation time step (s).

3.1.3 Objective function for model calibration

To simultaneously improve the simulation of near-natural reservoir inflow and human-regulated release, the average NSE (NSE_{ave}) was defined as the optimization objective.

$$\max \mathrm{NSE}_{\mathrm{ave}} = 1/2 \times (\mathrm{NSE}_{\mathrm{inflow}} + \mathrm{NSE}_{\mathrm{release}}) \tag{9}$$

where NSE_{inflow} and $NSE_{release}$ denote the NSE values for the simulated inflow and release, respectively. For a given time series, NSE is computed as

$$\mathrm{NSE} = 1 - \sum_{t=1}^{T} (Q_t^{\mathrm{sim}} - Q_t^{\mathrm{obs}})^2 / \sum_{t=1}^{T} (Q_t^{\mathrm{obs}} - \overline{Q}^{\mathrm{obs}})^2 \tag{10}$$

where Q_t^{sim} and Q_t^{obs} denote the simulated and observed streamflow at time t, respectively; $\overline{Q}^{\mathrm{obs}}$ is the mean observed streamflow over the evaluation period; and T is the total number of time steps. NSE ranges from $-\infty$ to 1, with 1 indicating a perfect match between simulated and observed streamflow. Although NSE tends to emphasize errors during high-flow periods because of its squared-error formulation, it was used here to calibrate overall inflow and release dynamics across the full flow regime. This choice supports the subsequent assessment of hydropower generation, and the power generation guarantee rate (Sect. 3.3). Hydrological drought conditions were evaluated separately using SSI and run-theory-based duration and severity metrics, and the remaining sensitivity to NSE-based calibration is discussed in Sect. 4.5.

3.2 Standardized streamflow index

This study used the standardized streamflow index (SSI) to characterize hydrological drought, because it only requires streamflow data and has been widely applied across a range of timescales, including 1-, 3-, 12-, and 24-month periods (Vicente-Serrano et al., 2012; Smith et al., 2019; Gu et al., 2020; Shukla and Wood, 2008). The 1-month (SSI-1) and 3-month (SSI-3) indices represent short-term hydrological conditions, whereas longer aggregation windows such as SSI-12 and SSI-24 reflect persistent, long-term hydrological drought conditions. Here, SSI-1, SSI-3, and SSI-12 were selected to represent monthly, seasonal, and annual hydrological drought, respectively.

In the calculation of SSI for each calendar month m (m = 1, 2, ..., 12) at a specific time scale, a Pearson type-III distribution was fitted to the corresponding aggregated streamflow series (Q) during the reference period. The goodness-of-fit was evaluated using the Kolmogorov–Smirnov test. The cumulative distribution function is expressed as:

$$F_m(Q) = \frac{\beta^{\alpha}}{\Gamma(\alpha)} \int_x^{\infty} (Q - \omega)^{\alpha - 1} e^{-\beta(Q-\omega)} \mathrm{d}r \tag{11}$$

where $F_m(Q)$ is the cumulative distribution function; α, β, and ω are the shape, scale, and location parameters of the

distribution, respectively, which were estimated using the L-moment method (Hosking, 1990). The SSI values were then obtained by applying the standard normal transformation (Φ^{-1}).

$$\mathrm{SSI} = \Phi^{-1}(F_m) \tag{12}$$

To ensure consistency in comparing hydrological drought characteristics between historical and future periods, the distribution parameters estimated from the 30-year reference period (1985–2014) were applied to the two future 30-year periods (i.e., the near-future and far-future) when computing SSI, following common practice in climate impact assessment studies (Yun et al., 2021b; Wan et al., 2018).

The characteristics (e.g., duration, severity, and intensity) of hydrological drought episodes were extracted using run theory (Yevjevich, 1967). A drought episode begins when SSI falls below a specific threshold (−0.5) and ends when SSI rises above the threshold, as illustrated by the two drought episodes D_0 and D_1 in Fig. 4. Drought duration is defined as the length of the drought episode, while drought severity is defined as the cumulative deficit of SSI values below the drought threshold during the episode. Drought intensity is defined as the average deficit below the threshold, calculated as severity divided by duration. In particular, two adjacent drought branches (d_0 and d_2) can be merged into a single drought episode (i.e., the third drought episode in Fig. 4) when the inter-event time d_1 is no longer than the time evaluation criterion t_c ($t_c = 2$ months in this study) and SSI remains below the allowable upper threshold during this interval (Zhou et al., 2021; Wu et al., 2017). Under this condition, the merged drought duration is calculated as $D_2 = d_0 + d_1 + d_2$ and the severity is $S_2 = s_0 + s_2$. Since drought intensity is defined as the ratio of severity to duration, only two drought characteristics, duration (D) and severity (S), are used in this study to comprehensively describe each drought episode.

3.3 Experimental Design

To systematically explore the roles of climate change and reservoir operation in shaping future hydrological droughts, a set of numerical experiments was designed (Table 2). Specifically, OBS/LSTM and OBS/LSTM+Reservoir denote simulations driven by observed CMA meteorological forcing, without and with reservoir operation, respectively. Similarly, ISIMIP3b_ref/LSTM and ISIMIP3b_ref/LSTM+Reservoir represent simulations driven by ISIMIP3b forcing during the reference period, without and with reservoir operation, respectively. The experiments ISIMIP3b_fut/LSTM and ISIMIP3b_fut/LSTM+Reservoir further incorporate future climate forcing to quantify the progressive impacts of climate change and reservoir operation on future projections. Notably, the term "Reservoir" in these experiments refers to the historical reservoir operation policy over 1992–2020, which was derived from the physics-guided LSTM model.

Little attention has been paid to the evolution of trade-offs between operating benefits and drought risks, although a large body of literature points out the necessity of optimizing reservoir operation policies (Ji et al., 2023; Brunner, 2021; Wu et al., 2022; Firoz et al., 2018). To this end, a classical multi-objective decision-making optimization was implemented for the Ankang Reservoir to maximize both hydropower generation and the power generation guarantee rate. The optimal set of alternative operating policies π_θ^* under historical climate conditions w^{H} was obtained by solving the following problem.

$$\begin{aligned}\pi_\theta^* &= \arg\max_{\pi_\theta} \boldsymbol{f}(\pi_\theta w^{\mathrm{H}}) \\ &= |\boldsymbol{f}_{\mathrm{THP}}(\pi_\theta w^{\mathrm{H}}), \boldsymbol{f}_{\mathrm{PGR}}(\pi_\theta w^{\mathrm{H}})|\end{aligned} \tag{13}$$

where $\boldsymbol{f}$ is the objective vector consisting of $[\boldsymbol{f}_{\mathrm{THP}} \boldsymbol{f}_{\mathrm{PGR}}]$ (see Sect. S2 for details). The operating policies π_θ were parameterized using Gaussian radial basis functions, which have been shown to be effective for reservoir operation optimization (Quinn et al., 2019; Bertoni et al., 2019). The optimization was performed using the Non-dominated Sorting Genetic Algorithm II (NSGA-II; Deb et al., 2002). The resulting Pareto-optimal policies, π_θ^*, were then applied under future climate scenarios to investigate the potential co-benefits and trade-offs between hydropower generation and drought risk reduction. This exploratory analysis corresponds to the ISIMIP3b_fut/LSTM+Reservoir_Opt experiment in Table 2, and detailed results are presented in Sect. 4.4.

4 Results and Discussion

4.1 Model calibration and validation

Figure 5 presents the calibration and validation results for both reservoir inflow and release using the LSTM-based modeling framework. As shown in Fig. 5a, the LSTM model reproduced the near-natural reservoir inflow well at the monthly scale, with NSE values of 0.95 and 0.93 for the calibration and validation periods, respectively. Figure 5b further evaluates the model performance across the full flow regime using flow duration curves (FDCs), showing that the simulated flow distribution generally follows the observed pattern across a wide range of exceedance probabilities. Figure 5c illustrates the comparison between observed and simulated reservoir release at the Ankang hydrological station. The seasonal shift between observed inflow and release curves (black lines in Fig. 5a and c) suggests that reservoir operations have reshaped streamflow seasonality, with an estimated 5 %–21 % of downstream flow withheld by the Ankang Reservoir during June–October and released later in the year. This operational pattern is well captured by the LSTM+Reservoir model driven by observed meteorological forcings, yielding NSE values of 0.91 and 0.89 for the calibration and validation

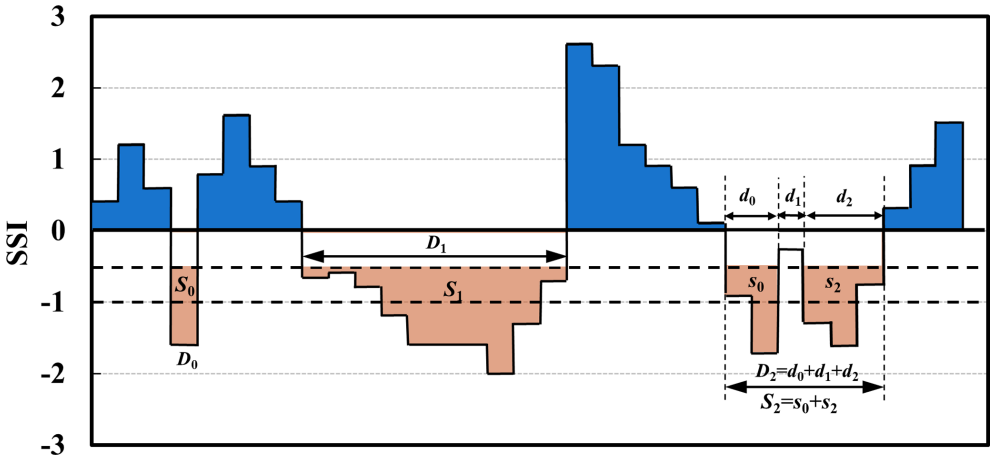

Figure 4. Identification of hydrological drought events and characteristics using run theory. Three types of drought episodes are illustrated in orange: episode D_0 with severity S_0, episode D_1 with severity S_1, and a merged episode D_2 with severity S_2, where $D_2 = d_0 + d_1 + d_2$ and $S_2 = s_0 + s_2$. The two adjacent drought branches d_0 and d_2 are merged when the interval d_1 is no longer than the time evaluation criterion t_c ($t_c = 2$ months in this study) and the SSI remains below the allowable upper threshold during d_1.

Table 2. Experimental design and scenario configurations used in this study.

Experiment	Meteorological forcing	Simulation period	Climate change	Traditional reservoir operation	Optimal reservoir operation
OBS/LSTM	Observations	1992–2020	–	–	–
OBS/LSTM + Reservoir	Observations	1992–2020	–	✓	–
ISIMIP3b_ref/LSTM	ISIMIP3b reference	1985–2014	–	–	–
ISIMIP3b_ref/LSTM +Reservoir	ISIMIP3b reference	1985–2014	–	✓	–
ISIMIP3b_fut/LSTM	ISIMIP3b future	2031–2060, 2071–2100	✓	–	–
ISIMIP3b_fut/LSTM +Reservoir	ISIMIP3b future	2031–2060, 2071–2100	✓	✓	–
ISIMIP3b_fut/LSTM +Reservoir_Opt	ISIMIP3b future	2031–2060, 2071–2100	✓	–	✓

periods, respectively. While slightly lower than those for inflow, these values reflect satisfactory performance given the complexity of human-influenced reservoir operations.

Figure 5a and c also show the ensemble-averaged hydrographs from the ISIMIP3b_ref/LSTM and ISIMIP3b_ref/LSTM+Reservoir experiments, driven by ISIMIP3b meteorological forcings rather than historical meteorological observations. The model performance under these forcings is noticeably weaker than that of the OBS/LSTM and OBS/LSTM+Reservoir configurations, likely due to limitations of ISIMIP3b in characterizing regional-scale meteorological regimes (Kang et al., 2023). FDCs in Fig. 5b and d further indicate that simulated low flows tend to be overestimated at high exceedance probabilities, which may affect the absolute magnitude of simulated low-flow conditions. Nevertheless, because subsequent analyses focus on changes relative to the ISIMIP3b_ref baseline, the influence of this systematic bias is likely to be attenuated. These simulations are therefore used for the subsequent hydrological drought analysis.

Changes in reservoir storage (ΔS) represent another key variable in our operation simulations and are also used in the hydropower performance assessment in Sect. 4.4. Figure 6 illustrates the observed and simulated mean monthly storage variations over the available period 2001–2010. Both the OBS/LSTM+Reservoir and ISIMIP3b_ref/LSTM+Reservoir simulations reproduce the observed dynamics well, particularly the storage accumula-

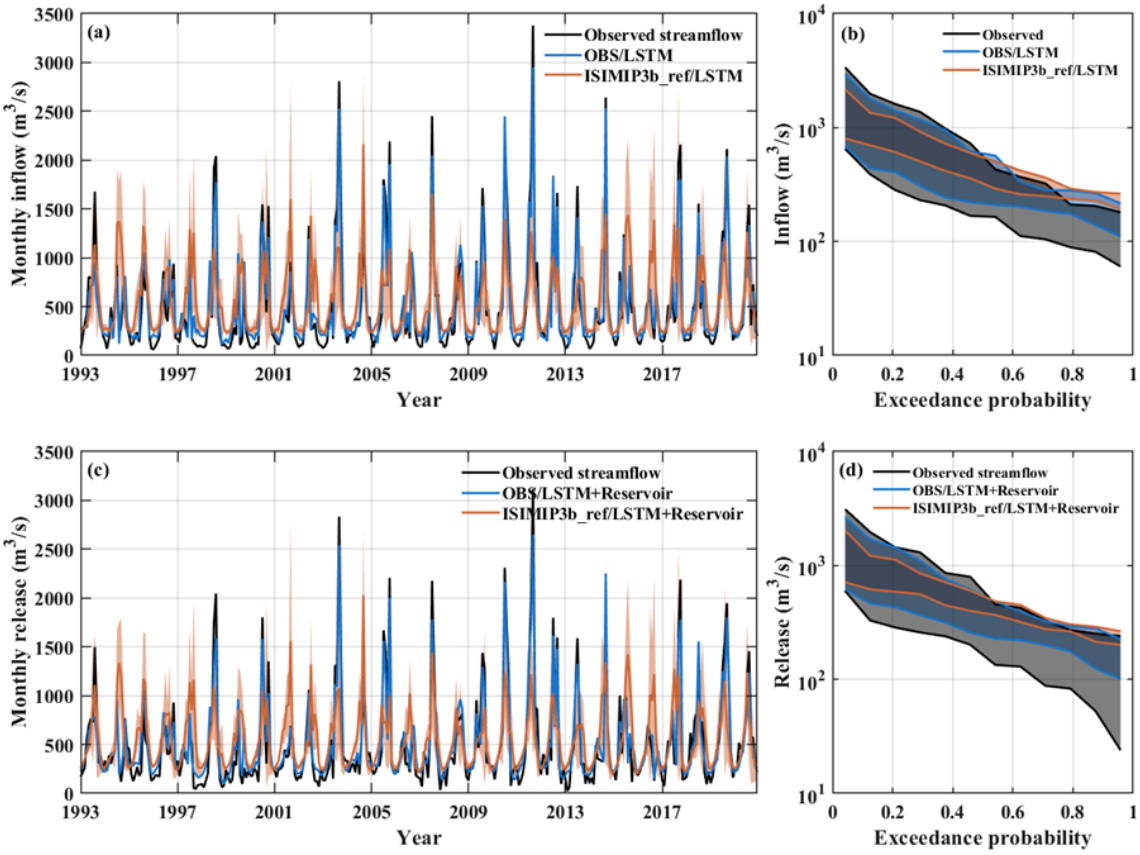

Figure 5. Evaluation of monthly reservoir inflow and release simulations. **(a, c)** Hydrographs of reservoir inflow and release; **(b, d)** Corresponding flow duration curves (FDCs). Simulations driven by meteorological observations (OBS/LSTM and OBS/LSTM+Reservoir) are marked as blue lines, while simulations driven by ISIMIP3b_ref forcings (ISIMIP3b_ref/LSTM and ISIMIP3b_ref/LSTM+Reservoir) are marked as orange lines. Shaded bands in **(a, c)** indicate the ensemble mean ±1 standard deviation of simulations driven by ISIMIP3b GCM forcings, while those in **(b, d)** denote the interannual range (min–max envelope) of annual FDCs.

tion from July to November. With correlation coefficients between simulated and observed storage series ranging from 0.70 to 0.73, the model provides a reasonable approximation of reservoir operations.

4.2 Streamflow variation under the influence of climate change and reservoir operation

ISIMIP3b climate projections indicate a consistent upward trend in both precipitation and temperature over the UHRB during future periods relative to the reference period (at a significance level of $p < 0.05$ based on the Mann-Kendall test). Among the SSP scenarios, SSP126 presents an increase in precipitation (+7.3 % to +13.3 %) and a modest temperature rise (+1.7 °C to +1.9 °C). SSP370 shows a similar increase in precipitation (+7.3 % to +11.2 %) but a more pronounced warming (+1.8 °C to +4.0 °C). Under SSP585, the largest increases are projected for both precipitation (+8.0 % to +15.8 %) and temperature (+2.3 °C to +5.3 °C). As a result of the combined climatic drivers, the multi-year average reservoir inflow is expected to increase from +0.3 % (near-future, 2031–2060) to +5.5 % (far-future, 2071–2100) under SSP126. Under SSP370 and SSP585, it is expected to shift from +0.2 % (near-future) to −7.0 % (far-future), and from −2.6 % (near-future) to −8.4 % (far-future), respectively, suggesting a potential long-term decline despite short-term gains. This implies that warming-induced evaporation losses may outweigh the compensating effects of increased precipitation, especially under higher-emission scenarios (Satoh et al., 2022).

Figure 7 further illustrates the projected relative change in monthly mean streamflow across future periods and SSP scenarios, explicitly highlighting the seasonal influence of both climate change and reservoir operation. Substantial inter-model uncertainty is evident, particularly under SSP585 during the far-future flood season, where streamflow changes range from −45 % to +43 %. Despite this variability, the ensemble mean reveals a consistent signal: positive deviations are mainly concentrated in the flood season, while most other months are expected to experience declining streamflow. This asymmetric seasonal response suggests an intensification of hydrological seasonality, with wetter periods

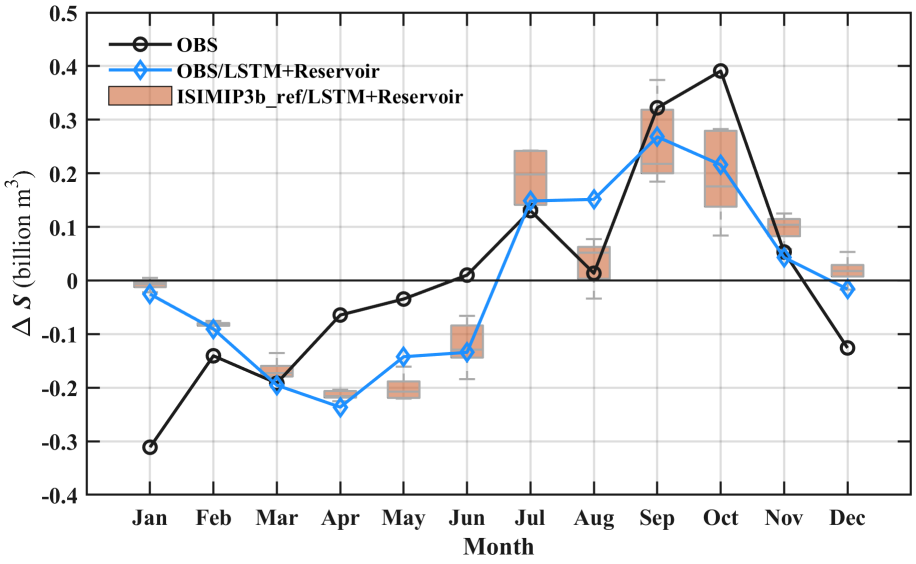

Figure 6. Mean monthly storage variations (ΔS) in the Ankang Reservoir during 2001–2010. The black dotted line represents the multi-year observations. The blue line shows the OBS/LSTM+Reservoir simulation. The orange boxplots represent the ISIMIP3b_ref/LSTM+Reservoir ensemble simulations driven by five ISIMIP3b GCMs.

becoming more flood-prone and drier periods experiencing heightened water stress. In general, human-regulated reservoir operation has the potential to moderate the magnitude of future monthly streamflow changes. However, across all scenarios, the extent to which the Ankang Reservoir alters streamflow patterns remains rather limited, which may be attributable to its primary operational objective of hydropower generation, with relatively little emphasis on shaping the flow regime itself. Further investigation into effective reservoir management is warranted.

4.3 Changes in hydrological drought events

To comprehensively evaluate future hydrological droughts, we analyzed both the continuous SSI-based drought characteristics and the annual drought event frequency and severity under different climate and reservoir operation scenarios. The time series of SSI-3 associated with reservoir inflow and release, together with their ensemble spreads under three emission scenarios, are shown in Fig. 8, with the SSI-1 and SSI-12 results provided in Figs. S1 and S2, respectively. SSI-1 and SSI-3 exhibit stronger short-term fluctuations within $[-3, 3]$, whereas SSI-12 shows smoother variability, reflecting more stable long-term dynamics. Consistent with the projected decreases in streamflow, all three indices (SSI-1, SSI-3, and SSI-12) show a slight worsening trend over time, particularly under SSP370 and SSP585, indicating an increased likelihood of drought occurrence in the future (Fig. 8b, d and f). We therefore quantified the number of drought events for three periods estimated by the GCMs and summarized them on the right side of Figs. 8, S1 and S2. Drought occurrence is generally higher in the future periods than in the reference period, despite substantial inter-model discrepancies across GCMs. The near-future period shows slightly more drought events than the far-future period, with more small and frequent droughts. In addition, as shown in Fig. 8b, d, and f, reservoir operation can reduce drought-event frequency in the reference period but does not completely remove the risk of hydrological drought under future climate change. Reservoir operation is better at preventing short-term droughts, as the drop in the number of droughts associated with reservoir release versus inflow is significant for SSI-1 in Fig. S1 but not for SSI-12 in Fig. S2. It may be related to the limited annual regulation capacity of the Ankang Reservoir.

A more comprehensive assessment of SSI-3 drought characteristics, including duration and severity, is provided in Fig. 9 (see Figs. S3 and S4 for SSI-1 and SSI-12, respectively). Both drought duration and severity are projected to increase under future climate change. The most extreme SSI-3 drought event is projected to occur in the far-future period under SSP585, with a maximum duration of 33 months and a maximum severity of 47.8. It is followed by SSP370, with an 18-month duration and a severity of 22.9, and finally SSP126, with a 12-month duration and a severity of 12.4. The drought duration and severity associated with SSI-1 and SSI-12 show a similar pattern. Overall, SSP585 exerts the most pronounced impact on hydrological drought in the region. Notably, reservoir operation substantially alleviates extreme hydrological drought by redistributing streamflow deficits through impoundment and release regulation. For the far-future period under SSP585, the maximum duration associated with SSI-3 is reduced by 72.73 % and the maximum severity is reduced by 63.81 % due to reservoir operation. A similar moderating effect is observed for SSI-1

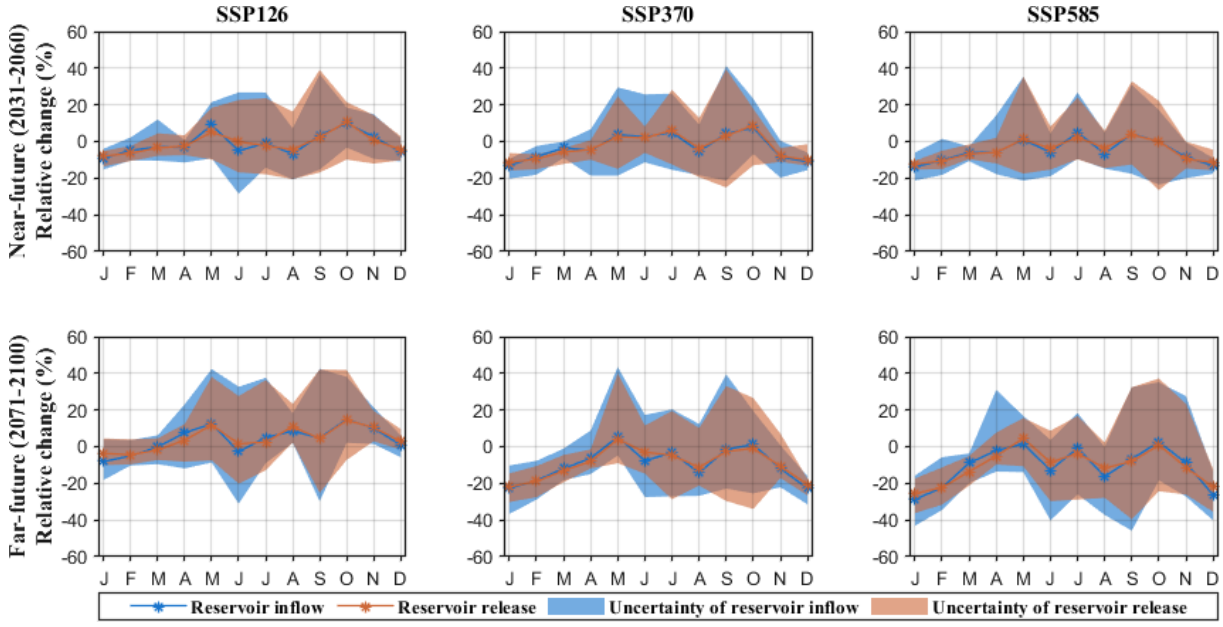

Figure 7. Relative changes in projected monthly reservoir inflow and release for two future periods and three SSP scenarios, relative to the reference period 1985–2014. Lines are the ensemble mean of the five GCMs, and shaded areas represent the uncertainty across the five GCMs.

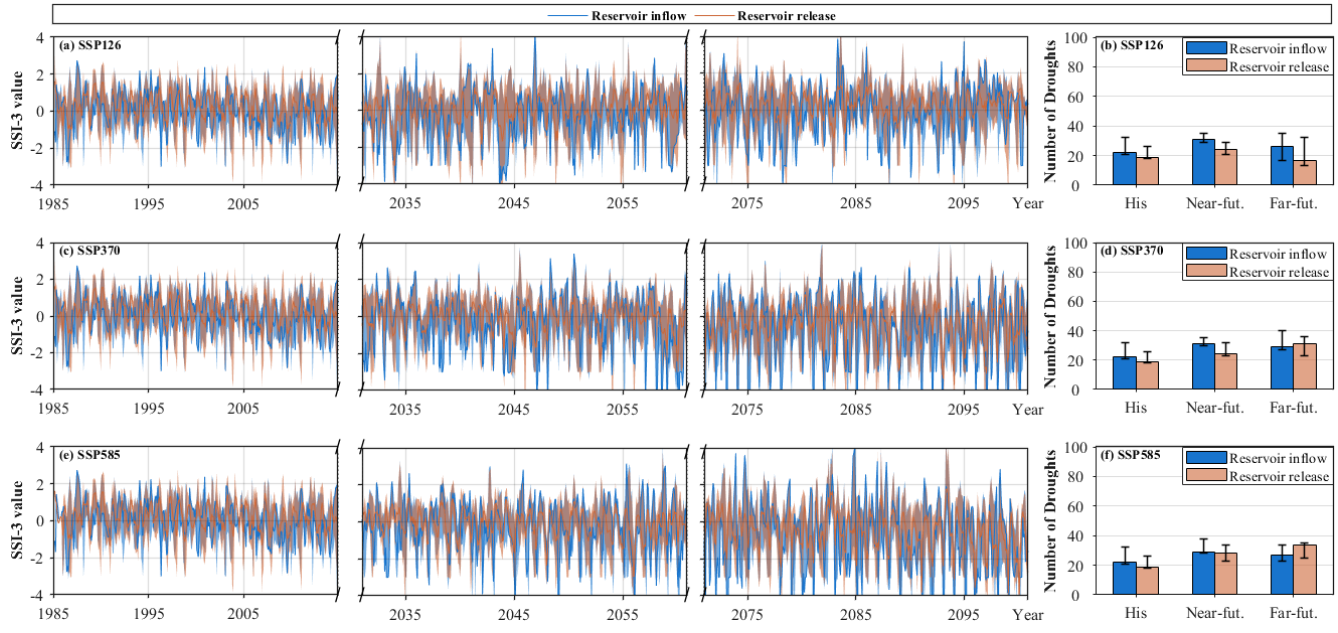

Figure 8. Hydrological drought SSI-3 for reference and future periods over the UHRB. **(a)** Time series of SSI-3 associated with reservoir inflow and release for the low-emission SSP126 scenario. Blue and orange intervals indicate their uncertainties, respectively. **(b)** Number of drought events for the reference period (1985–2014), near-future period (2031–2060), and far-future period (2071–2100). Colored bars are ensemble means and error bars represent the estimated difference in the number of drought events among the five GCMs. Panels **(c–f)** are the same as panels **(a)** and **(b)**, but for the medium-emission SSP370 and high-emission SSP585 scenarios, respectively.

(Fig. S3), yet the effect is less evident for SSI-12, suggesting that additional human interventions may be needed to mitigate long-term droughts.

4.4 Adaptability of optimal operating policies to future hydrological droughts

Optimal reservoir operating policies can serve as a potential adaptation measure to future climate change. Previous studies have highlighted their potential in mitigating the adverse impacts of severe hydrological events (Wu et al., 2023; Sun et al., 2023; Yun et al., 2021b; Levey and Sankarasubramanian, 2025). However, their practical validation remains limited. In this section, we applied the NSGA-II algorithm to derive 100 Pareto-optimal operating policies using historical inflow observations (Fig. 10), and examined their implications for future hydropower generation and drought characteristics under climate change.

The simulation results of these 100 optimal operating policies for hydropower generation and SSI-3 drought characteristics under future climate change conditions are shown in Fig. 11 as parallel-coordinate plots. The historically derived operating policy is outlined in black for comparison. These plots show each operating policy as a grey line that intersects each vertical axis at the achievable performance value, and the axes are oriented with the optimal direction upwards. The ideal policy in Fig. 11 is, therefore, a horizontal line across the top of each axis. Nevertheless, these lines usually intersect between adjacent axes because superior performance in one indicator comes at the cost of poorer performance in another. For instance, lower power generation guarantee rates inevitably constrain the goal of maximizing annual average hydropower generation. All optimal policies have similar future annual average hydropower generation, except for the far-future period under SSP126. They have a wide range of guarantee rates, such as 76.59 %–84.32 % for the near-future period under SSP126 and 61.07 %–72.05 % for the far-future period under SSP585. Additionally, as can be seen in all subplots of Fig. 11, all the optimal operating policies result in higher hydropower generation but also a higher drought frequency than the historically derived policy. The SSI-3 series associated with optimal reservoir release is broken into more drought events where the average duration and severity of droughts do not change substantially. The most challenging drought management task remains in the future-period under SSP585, during which the historically derived policy has the lowest drought severity. Overall, only a small number of optimal policies achieve robust and satisfactory performance of all considered indicators across plausible future scenarios, demonstrating their potential for mitigating short-term hydrological droughts.

4.5 Limitations, uncertainties, and implications

While the proposed framework provides a data-driven way to represent reservoir-regulated hydrological droughts under future climate scenarios, several limitations and sources of uncertainty should be explicitly acknowledged. These aspects are important for interpreting the robustness, scope, and broader applicability of our results.

i. *Possible non-stationarity of the operating environment and limited climate-model sampling.* In our framework, the physics-guided LSTM module learns reservoir operating behavior from historical conditions and is subsequently applied to the reference and future periods. This implicitly assumes that the governing operating objectives and constraints remain broadly stable, and that the learned decision logic is transferable across time. Our previous analyses indicate that, for the case investigated here, the reservoir-regulated hydrological response exhibits relatively stable patterns over multi-decadal timescales, supporting the feasibility of using a surrogate model to represent the whole-period operational behavior (He et al., 2023). However, such consistency is case-specific and may not hold in other basins where human interventions are stronger; caution is warranted when applying the proposed approach beyond the study basin. In addition, future projections are driven by a limited set of climate forcings (five ISIMIP3b GCMs), which may not fully span plausible hydroclimatic trajectories and extremes, thereby constraining the uncertainty range of the simulated drought responses. Key extensions include stress-testing surrogate transferability under plausible operational changes and quantifying climate-forcing uncertainty using a larger GCM ensemble.

ii. *Sensitivity of drought inferences to calibration choices and single-basin LSTM training.* Simulated hydrological drought characteristics can depend on the objective function adopted during model calibration (Knoben et al., 2019). In this study, calibration primarily relied on NSE, which tends to emphasize high-flow conditions at the expense of low-flow fidelity. This may affect drought assessments because, at the low-flow end of the flow regime (i.e., high exceedance probabilities), streamflow deficits play a dominant role in shaping drought onset, persistence, and severity. Consistent with this concern, the FDCs in Fig. 5b and d indicate a systematic high bias in low flows, implying that the absolute magnitude of drought intensity derived from simulated streamflow may be underestimated. Although our subsequent analyses focus on relative changes with respect to the ISIMIP3b_ref baseline, this sensitivity should be acknowledged. A more drought-facing calibration setup, e.g., low-flow-oriented objectives (log-

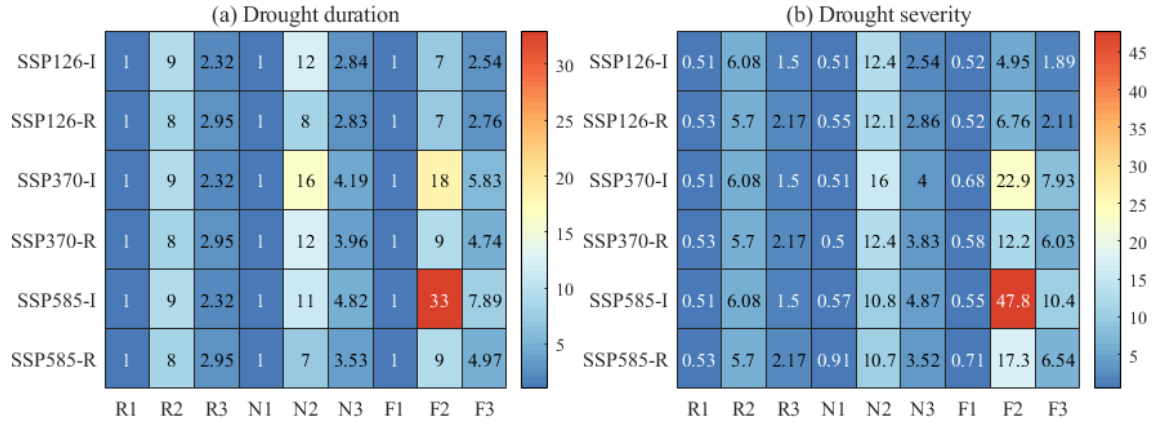

Figure 9. Heat map representation of **(a)** drought duration and **(b)** drought severity for the GCM-averaged SSI-3 series. The symbols R1, R2 and R3 indicate the minimum, maximum, and mean values during the reference period (1985–2014). N1, N2 and N3 are the same, but for the near-future period (2031–2060). F1, F2, and F3 are for the far-future period (2071–2100). Additionally, SSP126-I and SSP126-R are associated with reservoir inflow and release in the SSP126 scenario, SSP370-I and SSP370-R with the SSP370 scenario, and SSP585-I and SSP585-R with the SSP585 scenario.

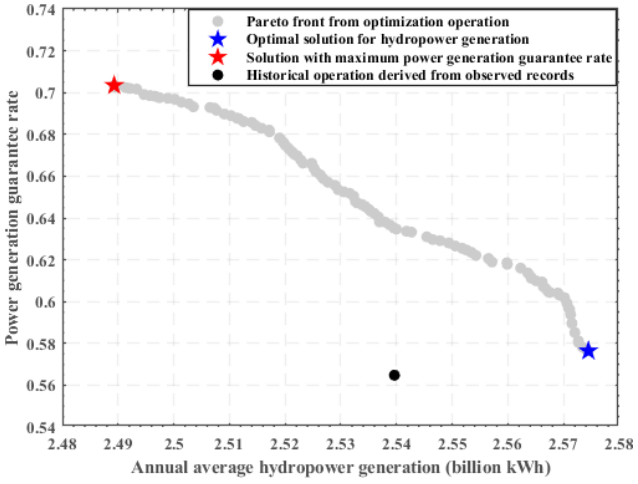

Figure 10. Trade-off between annual average hydropower generation and power generation guarantee rate for the Ankang Reservoir. Each grey dot represents an optimal operating policy identified using the NSGA-II algorithm, forming the Pareto front. The blue star marks the solution with the maximum hydropower generation, while the red star indicates the solution with the highest power generation guarantee rate. The black dot represents the historical operation derived from observed records.

transformed NSE), provides a direct path to reduce this sensitivity.

Beyond calibration, the physics-guided LSTM surrogate in our framework is trained using data from a single reservoir-regulated basin, which constrains the training envelope to the historical range of hydroclimatic and operational conditions represented in that system. This design choice was primarily motivated by limited access to harmonized reservoir operation records across regulated basins and by our focus on the target reservoir-regulated basin. Recent guidance for rainfall–runoff LSTM modeling highlights that single-basin training can limit generalization, particularly for extreme events, whereas multi-basin training on hydrologically diverse data is often more robust (Kratzert et al., 2024). As data availability permits, a natural extension is to conduct multi-basin (or multi-reservoir-system) training followed by fine-tuning on the target basin, and to explicitly evaluate how such training affects the simulation of drought-relevant low flows and extreme drought events.

iii. *Limitations of our optimized operating policy design.* Many reservoir optimization studies remain at a preliminary stage, where operating rules are optimized using historical observations and then deemed superior based solely on comparisons with historical performance. Although the observed historical operation, which is shaped by complex real-world objectives and constraints, is Pareto-dominated in the objective space of annual average hydropower generation and power-generation guarantee rate (Fig. 10), it is not necessarily outperformed by most Pareto-optimal policies under future scenarios, particularly in terms of guarantee rate and drought frequency (Fig. 11). In addition, a common challenge with Pareto-optimal solution sets is selecting a single implementable policy. By benchmarking the future performance of candidate Pareto solutions against the historical operating policy, we found that the reliability-oriented solution, that is, the one with the highest guarantee rate, performs better than the historical operating policy across most future scenarios, except for drought frequency, whereas the hydropower-optimal solution does not show consistent advantages. Hydropower generation is broadly

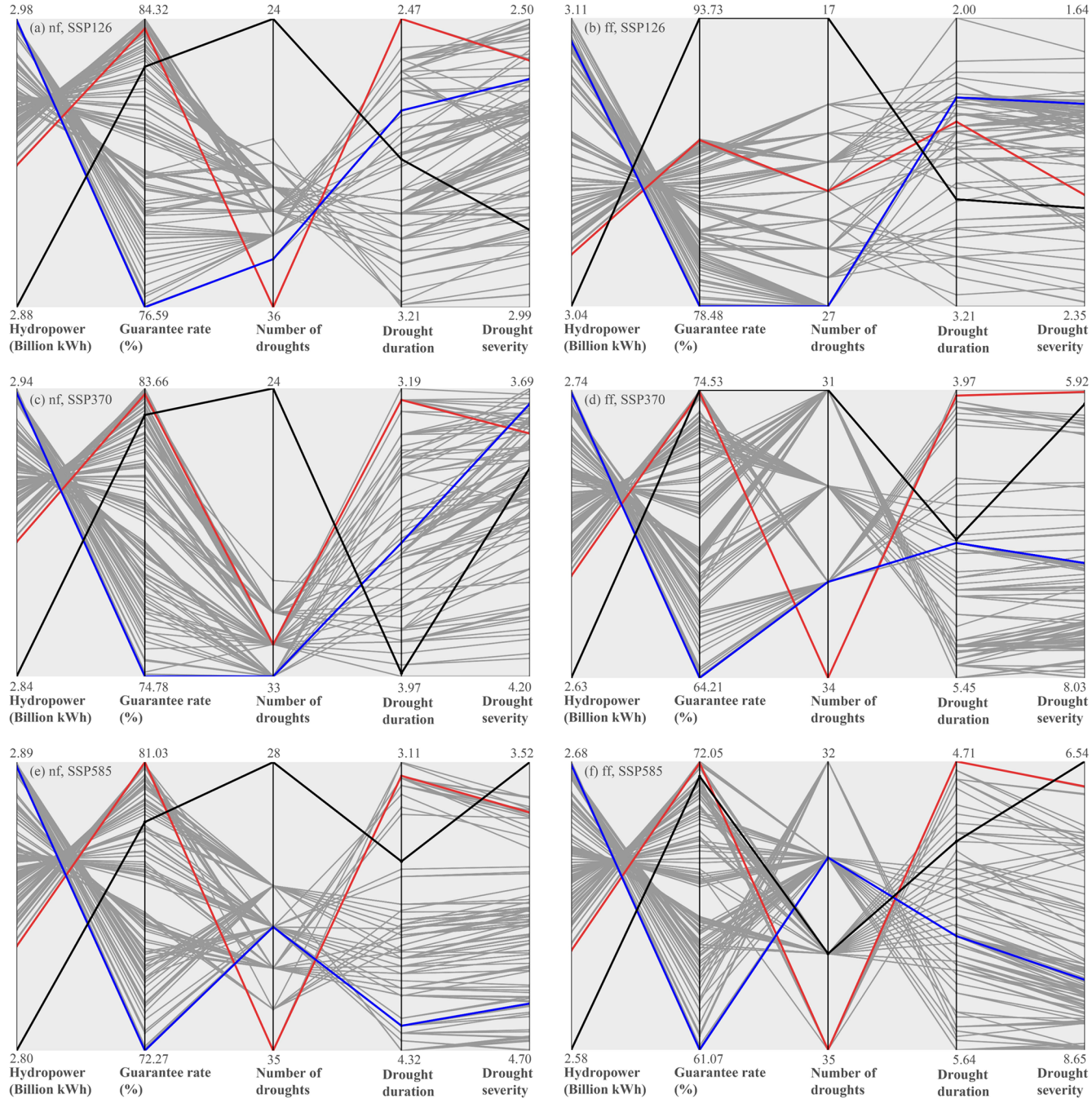

Figure 11. Trade-offs among hydropower generation, guarantee rate, and SSI-3 drought characteristics under optimal and historical reservoir operating policies using parallel coordinates plots. Panels **(a–b)** correspond to the near-future (nf) and far-future (ff) under SSP126, **(c–d)** under SSP370, and **(e–f)** under SSP585. The grey lines represent Pareto-optimal policies, while the red and blue lines indicate the solutions with the highest guarantee rate and maximum hydropower generation, respectively, and the black line indicates the historical operating pattern. Each axis represents an objective, with the optimal direction oriented upwards.

similar across the Pareto set in future periods, suggesting limited differentiation in this metric. These findings together suggest that for the Ankang system, the reliability-oriented solution is a more defensible candidate for implementation. Additionally, the optimized policies in our drought-focused analysis were derived primarily for hydropower generation and power generation guarantee rate and were then directly applied to future scenarios to examine trade-offs with hydrological drought mitigation. This indicates room for fur-

ther improvements in drought mitigation performance. Future work could incorporate drought-event characteristics as explicit objectives or constraints, and consider other human interventions (e.g., inter-basin water transfers and urbanization) to better bracket plausible drought-mitigation pathways under changing conditions (Wu et al., 2023; Firoz et al., 2018).

5 Conclusions

By coupling an LSTM-based reservoir inflow model with a physics-guided reservoir operation model, this study developed a fully automated ML-based framework to project streamflow changes over the UHRB under different future scenarios and associated hydrological droughts. The effects of climate change and reservoir operation were considered sequentially to reveal their different roles. Additionally, the trade-off between future hydrological droughts and operating benefits (i.e., hydropower generation and power generation guarantee rate) was investigated by optimizing the reservoir operating policies. The main findings are summarized as follows:

1. A reasonable LSTM-based model architecture is recommended for hydrological simulation in the reservoir-regulated region. When ISIMIP3b historical meteorological forcing is used instead of observed meteorological forcing, the model can still reproduce the inflow and release of the Ankang Reservoir, as well as changes in reservoir storage. This demonstrates the feasibility of projecting future streamflow and associated hydrological droughts using ML approaches.

2. Future climate change over the UHRB is projected to reduce natural streamflow and exacerbate hydrological droughts, especially in the far-future period (2071–2100) under the SSP585 scenario. While the operation of the Ankang Reservoir can mitigate the frequency, duration, and severity of short-term hydrological droughts (SSI-1 and SSI-3), it shows limited effectiveness in alleviating long-term droughts (SSI-12).

3. The optimal reservoir operating policies at Ankang Reservoir, designed to maximize hydropower generation and power generation guarantee rates, highlight clear trade-offs between hydrological drought risk and hydropower benefits under future climate scenarios. Compared with the historically derived policy, these optimal strategies yield higher hydropower benefits but may also lead to increased drought frequency. The finding that a small subset of optimal policies consistently delivers robust performance across multiple indicators under plausible future scenarios underscores the potential of these policies to enhance regional water resources management under climate change.

Code and data availability. The code that supports the findings of this study is available from the corresponding author upon reasonable request. The ISIMIP3b data used in producing this paper are available at https://data.isimip.org/search/tree/ISIMIP3b/InputData/ (last access: 23 May 2025). Observed streamflow data are available from the Bureau of Hydrology of the Yangtze Water Resources Commission of China (https://www.cjh.com.cn, last access: 23 May 2025).

Supplement. The supplement related to this article is available online at https://doi.org/10.5194/hess-30-3529-2026-supplement.

Author contributions. YG, KC and SH designed the study. SH, SS, and YL developed the models, with SH and LZ implementing them. SH drafted the manuscript in close collaboration with YG, SS, YL contributed to the data curation. Throughout the study period, all the authors engaged in discussions regarding the results, provided critical feedback, and approved the final version of the paper.

Competing interests. The contact author has declared that none of the authors has any competing interests.

Disclaimer. Publisher's note: Copernicus Publications remains neutral with regard to jurisdictional claims made in the text, published maps, institutional affiliations, or any other geographical representation in this paper. The authors bear the ultimate responsibility for providing appropriate place names. Views expressed in the text are those of the authors and do not necessarily reflect the views of the publisher.

Acknowledgements. We are very grateful to the editors and reviewers for their valuable comments, which could greatly improve the quality of the paper.

Financial support. This research has been supported by the National Key Research and Development Program of China (grant no. 2023YFC3209502), National Natural Science Foundation of China (grant nos. U2340217, 42577102 and 52595704), and the Basic Research Program of Jiangsu (grant no. BK20250013).

Review statement. This paper was edited by Keirnan Fowler and reviewed by Andrew John and one anonymous referee.

References

Abadi, M., Barham, P., Chen, J., Chen, Z., and Davis, A.: TensorFlow: a system for large-scale machine learning, in: Proceedings of the 12th USENIX conference on Operating Systems Design and Implementation, USENIX Association, Savannah, GA, USA, 265–283, https://www.usenix.org/conference/

osdi16/technical-sessions/presentation/abadi (last access: 23 May 2025), 2016.

Arsenault, R., Martel, J.-L., Brunet, F., Brissette, F., and Mai, J.: Continuous streamflow prediction in ungauged basins: long short-term memory neural networks clearly outperform traditional hydrological models, Hydrol. Earth Syst. Sci., 27, 139–157, https://doi.org/10.5194/hess-27-139-2023, 2023.

Bertoni, F., Castelletti, A., Giuliani, M., and Reed, P. M.: Discovering Dependencies, Trade-Offs, and Robustness in Joint Dam Design and Operation: An Ex-Post Assessment of the Kariba Dam, Earth's Future, 7, 1367–1390, https://doi.org/10.1029/2019ef001235, 2019.

Brunner, M. I.: Reservoir regulation affects droughts and floods at local and regional scales, Environ. Res. Lett., 16, 124016, https://doi.org/10.1088/1748-9326/ac36f6, 2021.

Chai, Y., Yue, Y., Slater, L. J., Yin, J., Borthwick, A. G. L., Chen, T., and Wang, G.: Constrained CMIP6 projections indicate less warming and a slower increase in water availability across Asia, Nat. Commun., 13, 4124, https://doi.org/10.1038/s41467-022-31782-7, 2022.

Chang, L., Cheng, L., Zhang, L., Han, D., Zhang, J., and Liu, P.: Remote sensing-based high-resolution reservoir drought index for identifying the occurrence and propagation of hydrological droughts in a large river basin, Remote Sens. Environ., 328, 114859, https://doi.org/10.1016/j.rse.2025.114859, 2025.

Chen, E. and Yu, X.: A transferable machine learning model for real-time forecast of epidemic dynamics and pre-trigger event warning, Ai Civ. Eng., 4, 18, https://doi.org/10.1007/s43503-025-00059-5, 2025.

Cheng, H., Wang, T., and Yang, D.: Quantifying the Regulation Capacity of the Three Gorges Reservoir on Extreme Hydrological Events and Its Impact on Flow Regime in a Changing Climate, Water Resour. Res., 60, e2023WR036329, https://doi.org/10.1029/2023wr036329, 2024.

Cui, Z., Zhou, Y., Guo, S., Wang, J., and Xu, C.-Y.: Effective improvement of multi-step-ahead flood forecasting accuracy through encoder-decoder with an exogenous input structure, J. Hydrol., 609, 127764, https://doi.org/10.1016/j.jhydrol.2022.127764, 2022.

Culley, S., Noble, S., Yates, A., Timbs, M., Westra, S., Maier, H. R., Giuliani, M., and Castelletti, A.: A bottom-up approach to identifying the maximum operational adaptive capacity of water resource systems to a changing climate, Water Resour. Res., 52, 6751–6768, https://doi.org/10.1002/2015wr018253, 2016.

Dams, C. N. C. o. L.: Ankang hydropower project, Beijing: Chinese National Committee on Large Dams, http://www.chincold.org.cn/dams/index.htm (last access: 23 May 2025), 2011 (in Chinese).

Deb, K., Pratap, A., Agarwal, S., and Meyarivan, T.: A fast and elitist multiobjective genetic algorithm: NSGA-II, IEEE Trans. Evol. Comput., 6, 182–197, https://doi.org/10.1109/4235.996017, 2002.

Eriyagama, N., Smakhtin, V., and Udamulla, L.: How much artificial surface storage is acceptable in a river basin and where should it be located: A review, Earth-Sci. Rev., 208, 103294, https://doi.org/10.1016/j.earscirev.2020.103294, 2020.

Firoz, A. B. M., Nauditt, A., Fink, M., and Ribbe, L.: Quantifying human impacts on hydrological drought using a combined modelling approach in a tropical river basin in central Vietnam, Hydrol. Earth Syst. Sci., 22, 547–565, https://doi.org/10.5194/hess-22-547-2018, 2018.

G. Ribeiro Neto, G., Kchouk, S., Melsen, L. A., Cavalcante, L., Walker, D. W., Dewulf, A., Costa, A. C., Martins, E. S. P. R., and van Oel, P. R.: HESS Opinions: Drought impacts as failed prospects, Hydrol. Earth Syst. Sci., 27, 4217–4225, https://doi.org/10.5194/hess-27-4217-2023, 2023.

García-Feal, O., González-Cao, J., Fernández-Nóvoa, D., Astray Dopazo, G., and Gómez-Gesteira, M.: Comparison of machine learning techniques for reservoir outflow forecasting, Nat. Hazards Earth Syst. Sci., 22, 3859–3874, https://doi.org/10.5194/nhess-22-3859-2022, 2022.

Gu, L., Chen, J., Yin, J., Xu, C. Y., and Zhou, J.: Responses of precipitation and runoff to climate warming and implications for future drought changes in China, Earth's Future, 8, e2020EF001718, https://doi.org/10.1029/2020ef001718, 2020.

Gudmundsson, L., Boulange, J., Do, H. X., Gosling, S. N., Grillakis, M. G., Koutroulis, A. G., Leonard, M., Liu, J., Müller Schmied, H., Papadimitriou, L., Pokhrel, Y., Seneviratne, S. I., Satoh, Y., Thiery, W., Westra, S., Zhang, X., and Zhao, F.: Globally observed trends in mean and extreme river flow attributed to climate change, Science, 371, 1159–1162, https://doi.org/10.1126/science.aba3996, 2021.

Hanasaki, N., Kanae, S., and Oki, T.: A reservoir operation scheme for global river routing models, J. Hydrol., 327, 22–41, https://doi.org/10.1016/j.jhydrol.2005.11.011, 2006.

He, S., Guo, S., Zhang, J., Liu, Z., Cui, Z., Zhang, Y., and Zheng, Y.: Multi-objective operation of cascade reservoirs based on short-term ensemble streamflow prediction, J. Hydrol., 610, 127936, https://doi.org/10.1016/j.jhydrol.2022.127936, 2022.

He, S., Chen, K., Liu, Z., and Deng, L.: Exploring the impacts of climate change and human activities on future runoff variations at the seasonal scale, J. Hydrol., 619, 129382, https://doi.org/10.1016/j.jhydrol.2023.129382, 2023.

He, S., Li, B., Li, Q., Zheng, H., and Chen, Y.: Refining hydropower operation by dynamic control of cascade reservoir water levels with flood season segmentation, Energy, 314, 134156, https://doi.org/10.1016/j.energy.2024.134156, 2025.

Ho, S. Q.-G. and Ehret, U.: Is drought protection possible without compromising flood protection? Estimating the potential dual-use benefit of small flood reservoirs in southern Germany, Hydrol. Earth Syst. Sci., 29, 2785–2810, https://doi.org/10.5194/hess-29-2785-2025, 2025.

Hochreiter, S.: The Vanishing Gradient Problem During Learning Recurrent Neural Nets and Problem Solutions, Int. J. Uncertain. Fuzziness Knowlege-Based Syst., 06, 107–116, https://doi.org/10.1142/s0218488598000094, 1998.

Hochreiter, S. and Schmidhuber, J.: Long short-term memory, Neural Comput., 9, 1735–1780, https://doi.org/10.1162/neco.1997.9.8.1735, 1997.

Hosking, J. R. M.: L-Moments: Analysis and estimation of distributions using linear combinations of order statistics, J. R. Stat. Soc. Ser. B Methodol., 52, 105–124, https://doi.org/10.1111/j.2517-6161.1990.tb01775.x, 1990.

Huang, J., Sangiorgio, M., Wu, W., Maier, H. R., Wang, Q. J., Hughes, J., and Castelletti, A.: Solving the robustness puzzle: The joint impact of optimization approach, robustness metrics, and scenarios on water resources management

under deep uncertainty, J. Environ. Manag., 373, 123540, https://doi.org/10.1016/j.jenvman.2024.123540, 2025.

Huang, J., Wu, W., Maier, H. R., Hughes, J., Wang, Q. J., and Cao, Y.: Comprehensive framework for long-term reservoir management under deep uncertainty, Environ. Modell. Softw., 195, 106740, https://doi.org/10.1016/j.envsoft.2025.106740, 2026.

IPCC: The Physical Science Basis, Contribution of Working Group I to the Sixth Assessment Report of the Intergovernmental Panel on Climate Change, Cambridge University Press, https://doi.org/10.1017/9781009157896 2021.

Ji, P., Yuan, X., and Jiao, Y.: Future hydrological drought changes over the upper Yellow River basin: The role of climate change, land cover change and reservoir operation, J. Hydrol., 617, 129128, https://doi.org/10.1016/j.jhydrol.2023.129128, 2023.

Jin, H., Willems, P., Chen, X., and Liu, M.: Nonstationary flood and its influencing factors analysis in the Hanjiang River Basin, China, J. Hydrol., 625, 129994, https://doi.org/10.1016/j.jhydrol.2023.129994, 2023.

Kang, S., Yin, J., Gu, L., Yang, Y., Liu, D., and Slater, L.: Observation-constrained projection of flood risks and socioeconomic exposure in China, Earth's Future, 11, e2022EF003308, https://doi.org/10.1029/2022ef003308, 2023.

Kheyruri, Y., Sharafati, A., and Neshat, A.: The socioeconomic impact of severe droughts on agricultural lands over different provinces of Iran, Agric. Water Manag., 289, 108550, https://doi.org/10.1016/j.agwat.2023.108550, 2023.

Kingma, D. P. and Ba, J.: Adam: a method for stochastic optimization, arXiv [preprint], https://arxiv.org/abs/1412.6980 (23 May 2025), 2014.

Knoben, W. J. M., Freer, J. E., and Woods, R. A.: Technical note: Inherent benchmark or not? Comparing Nash–Sutcliffe and Kling–Gupta efficiency scores, Hydrol. Earth Syst. Sci., 23, 4323–4331, https://doi.org/10.5194/hess-23-4323-2019, 2019.

Kratzert, F., Gauch, M., Klotz, D., and Nearing, G.: HESS Opinions: Never train a Long Short-Term Memory (LSTM) network on a single basin, Hydrol. Earth Syst. Sci., 28, 4187–4201, https://doi.org/10.5194/hess-28-4187-2024, 2024.

Lange, S.: Trend-preserving bias adjustment and statistical downscaling with ISIMIP3BASD (v1.0), Geosci. Model Dev., 12, 3055–3070, https://doi.org/10.5194/gmd-12-3055-2019, 2019.

Levey, J. R. and Sankarasubramanian, A.: Is Reservoir Storage Effectively Utilized in the Southeastern US? A Regional Assessment to Improve Water Supply Availability Considering Potential Storage and Flood Scenarios, Earth's Future, 13, e2024EF005176, https://doi.org/10.1029/2024ef005176, 2025.

Liu, J., Yuan, X., Zeng, J., Jiao, Y., Li, Y., Zhong, L., and Yao, L.: Ensemble streamflow forecasting over a cascade reservoir catchment with integrated hydrometeorological modeling and machine learning, Hydrol. Earth Syst. Sci., 26, 265–278, https://doi.org/10.5194/hess-26-265-2022, 2022.

Longyang, Q. and Zeng, R.: A Hierarchical Temporal Scale Framework for Data-Driven Reservoir Release Modeling, Water Resour. Res., 59, e2022WR033922, https://doi.org/10.1029/2022wr033922, 2023.

Özdoğan-Sarıkoç, G., Sarıkoç, M., Celik, M., and Dadaser-Celik, F.: Reservoir volume forecasting using artificial intelligence-based models: Artificial Neural Networks, Support Vector Regression, and Long Short-Term Memory, J. Hydrol., 616, 128766, https://doi.org/10.1016/j.jhydrol.2022.128766, 2023.

Quinn, J. D., Reed, P. M., Giuliani, M., and Castelletti, A.: What is controlling our control rules? Opening the black box of multireservoir operating policies using time-varying sensitivity analysis, Water Resour. Res., 55, 5962–5984, https://doi.org/10.1029/2018wr024177, 2019.

Rehana, S. and Rajesh, M.: Assessment of impacts of climate change on Indian riverine thermal regimes using hybrid deep learning methods, Water Resour. Res., 59, e2021WR031347, https://doi.org/10.1029/2021wr031347, 2023.

Satoh, Y., Yoshimura, K., Pokhrel, Y., Kim, H., Shiogama, H., Yokohata, T., Hanasaki, N., Wada, Y., Burek, P., Byers, E., Schmied, H. M., Gerten, D., Ostberg, S., Gosling, S. N., Boulange, J. E. S., and Oki, T.: The timing of unprecedented hydrological drought under climate change, Nat. Commun., 13, 3287, https://doi.org/10.1038/s41467-022-30729-2, 2022.

Shukla, S. and Wood, A. W.: Use of a standardized runoff index for characterizing hydrologic drought, Geophys. Res. Lett., 35, L02405, https://doi.org/10.1029/2007gl032487, 2008.

Smith, K. A., Barker, L. J., Tanguy, M., Parry, S., Harrigan, S., Legg, T. P., Prudhomme, C., and Hannaford, J.: A multi-objective ensemble approach to hydrological modelling in the UK: an application to historic drought reconstruction, Hydrol. Earth Syst. Sci., 23, 3247–3268, https://doi.org/10.5194/hess-23-3247-2019, 2019.

Solanki, H., Vegad, U., Kushwaha, A., and Mishra, V.: Improving Streamflow Prediction Using Multiple Hydrological Models and Machine Learning Methods, Water Resour. Res., 61, e2024WR038192, https://doi.org/10.1029/2024wr038192, 2025.

Sun, J., Chen, W., Hu, B., Xu, Y. J., Zhang, G., Wu, Y., Hu, B., and Song, Z.: Roles of reservoirs in regulating basin flood and droughts risks under climate change: Historical assessment and future projection, J. Hydrol.: Reg. Stud., 48, 101453, https://doi.org/10.1016/j.ejrh.2023.101453, 2023.

Tran, H., Zhou, T., Tan, Z., Fang, Y., and Ruby Leung, L.: Improving the prediction of daily reservoir releases over the CONUS using conditioned LSTM, J. Hydrol., 661, 133750, https://doi.org/10.1016/j.jhydrol.2025.133750, 2025.

Vicente-Serrano, S. M., Lopez-Moreno, J. I., Begueria, S., Lorenzo-Lacruz, J., Azorin-Molina, C., and Moran-Tejeda, E.: Accurate computation of a streamflow drought index, J. Hydrol. Eng., 17, 318–332, https://doi.org/10.1061/(Asce)He.1943-5584.0000433, 2012.

Wan, W., Zhao, J., Li, H. Y., Mishra, A., Hejazi, M., Lu, H., Demissie, Y., and Wang, H.: A holistic view of water management impacts on future Droughts: A Global Multimodel Analysis, J. Geophys. Res. Atmos., 123, 5947–5972, https://doi.org/10.1029/2017jd027825, 2018.

Wan, W., Wang, Z., Cheng, L., Bai, Y., Wang, W., and Wang, K.: Integrating Drought Warning Water Level With Analytical Hedging for Reservoir Water Supply Operation, Water Resour. Res., 61, e2024WR038680, https://doi.org/10.1029/2024wr038680, 2025.

Wanders, N. and Wada, Y.: Human and climate impacts on the 21st century hydrological drought, J. Hydrol., 526, 208–220, https://doi.org/10.1016/j.jhydrol.2014.10.047, 2015.

Wu, G., Chen, J., Shi, X., Kim, J. S., Xia, J., and Zhang, L.: Impacts of global climate warming on meteorological and hydrological droughts and their propagations, Earth's Future, 10, e2021EF002542, https://doi.org/10.1029/2021ef002542, 2022.

Wu, J., Chen, X., Yao, H., Gao, L., Chen, Y., and Liu, M.: Non-linear relationship of hydrological drought responding to meteorological drought and impact of a large reservoir, J. Hydrol., 551, 495–507, https://doi.org/10.1016/j.jhydrol.2017.06.029, 2017.

Wu, Y., Sun, J., Hu, B., Xu, Y. J., Rousseau, A. N., and Zhang, G.: Can the combining of wetlands with reservoir operation reduce the risk of future floods and droughts?, Hydrol. Earth Syst. Sci., 27, 2725–2745, https://doi.org/10.5194/hess-27-2725-2023, 2023.

Yang, S., Yang, D., Chen, J., and Zhao, B.: Real-time reservoir operation using recurrent neural networks and inflow forecast from a distributed hydrological model, J. Hydrol., 579, 124229, https://doi.org/10.1016/j.jhydrol.2019.124229, 2019.

Yevjevich, V.: An objective approach to definitions and investigation of continental hydrologic droughts, Hydrology Paper 23, Fort Collins, Colorado State U., http://hdl.handle.net/10217/61303 (last access: 23 May 2025), 1967.

Yun, X., Tang, Q., Sun, S., and Wang, J.: Reducing Climate Change Induced Flood at the Cost of Hydropower in the Lancang-Mekong River Basin, Geophys. Res. Lett., 48, e2021GL094243, https://doi.org/10.1029/2021gl094243, 2021a.

Yun, X., Tang, Q., Li, J., Lu, H., Zhang, L., and Chen, D.: Can reservoir regulation mitigate future climate change induced hydrological extremes in the Lancang-Mekong River Basin?, Sci. Total Environ., 785, https://doi.org/10.1016/j.scitotenv.2021.147322, 2021b.

Zhang, X., Song, Z., Zhou, T., Wang, D., Wang, Y., and Liu, P.: Reservoir operation strategies to mitigate hydrological drought effects along the middle and lower reaches of the Yangtze River, J. Hydrol.: Reg. Stud., 58, 102204, https://doi.org/10.1016/j.ejrh.2025.102204, 2025.

Zheng, Y., Liu, P., Cheng, L., Xie, K., Lou, W., Li, X., Luo, X., Cheng, Q., Han, D., and Zhang, W.: Extracting operation behaviors of cascade reservoirs using physics-guided long-short term memory networks, J. Hydrol.: Reg. Stud., 40, 101034, https://doi.org/10.1016/j.ejrh.2022.101034, 2022.

Zhou, Z., Shi, H., Fu, Q., Ding, Y., Li, T., and Liu, S.: Investigating the propagation from meteorological to hydrological drought by introducing the nonlinear dependence with directed information transfer index, Water Resour. Res., 57, e2021WR030028, https://doi.org/10.1029/2021wr030028, 2021.